Voltammetric sensitivity enhancement by using pre-concentration adjacent to the electrode: simulation, critical evaluation, and insights

Shaltiel Eloul and Richard G. Compton*

Department of Chemistry, Physical & Theoretical Chemistry Laboratory Oxford University, South Parks Road, Oxford OX1 3QZ (UK)

E-mail: richard.compton@chem.ox.ac.uk

Phone: +44 (0)1865 277389. Fax: +44 (0) 1865 275957

KEYWORDS: Voltammetry, pre-concentration, cyclic voltammetry, modified electrode, adsorption, nanoparticle voltammetry.

*To whom correspondence should be addressed

Abstract

A popular approach to enhancing the sensitivity of voltammetry is the surface modification of electrodes so as to provide adsorption sites which allow pre-concentration of target species, so as to promote sensitivity and reduced limits of detection. The surface modifier is typically inert other than providing enhanced adsorption and hence pre-concentration and non-conductive so that after pre-concentration the adsorbent must desorb and diffuse to the electrode before detection. We report the simulation of an idealized model for this type of voltammetry, focusing in particular on the effects of adsorption coverage and binding strength on the surface on the voltammetry response.

Introduction

Chemically modified electrodes have found enormous application in electrochemistry following the pioneering work of Murray and colleagues.[1–4] In one recent and popular variant the electrode is modified with insulating particles, often nanoparticles, which serve to enhance voltammetry signals by means of pre-concentrating target species prior to voltammetric detection. Table 1 provides a range of illustrative examples.[5–15] The approach for particular analytes is generally developed empirically. The aim of the present paper is to explore the parameters underpinning the method using an idealized model. In particular it can be anticipated that the two step process in which adsorption on particles or surfaces adjacent to the detection electrode prior to voltammetry requires the subsequent desorption and diffusion of the target to the electrode. It follows then that the strategy requires a delicate balance of adsorption strength in order to be useful. In particular very strong irreversible adsorption will simply provide a 'sink' for the analyte and no useful signals, whilst slow adsorption and/or slow desorption will be similarly useless. In order to probe the balance, we adopt the idealized model shown in figure 1. Here we consider a disc electrode surrounded by a concentric ring ('sheath') on which adsorption occurs exclusively. We allow the latter to pre-concentrate the target analyte, A. After the pre-concentration, we explore via simulation the

effect on the voltammetry of species A at the disc electrode. In this way the thermodynamics and kinetics of the process:

$$A(aq) \leftrightarrows A(ads) \tag{1}$$

are shown to strongly influence the current response only under very carefully selected conditions.

Previously, we reported that the supporting sheath surrounding a micro-disc electrode can significantly shield the current response when the electro-active species irreversibly adsorbs on the surface.[16] It was found that in case of irreversible adsorption on the supporting sheath, the measured current is reduced reflecting the adsorbing rate and the radius ratio between the disc and the surface. This shielding effect was also discussed in nanoparticle impact analysis[17] and other evidence of 'shielding' has been noted.[18,19] Following that, in this study, new interest has arisen in studying the case where a *reversible* adsorption takes place on the surface surrounding an electrode as a model for the chemically modified electrodes described above. Transient voltammetry measurements such as cyclic voltammetry (CV) can be dramatically affected by this adsorbing surface, since, when scanning the potential, a diffusional transport of material towards or away from the disc electrode changes of concentration distribution in the cell local to the electrode which can potentially trigger desorption of material from the surface towards the electrode.

This study reveals new insights of how electrochemical behaviour can be influenced by the surface surrounding a disc electrode and underpinning sensitive analytical methods and applications related to physical adsorption of nanoparticles or molecules on modified surfaces (see Table 1). Additionally, the basic understanding of how an adjacent surface can control the behaviour of the voltammetry, provides a novel way to make responsive controlled released electrochemical systems and high sensitive detection.[20,21] For example, it can boosts the Faraday current when the concentration drops in the solution near the electrode, or releasing particles of interest from the surface to the solution when a reaction on the disc electrode occurs.

In this work, we report the effect of an annular sheath concentric with a working electrode as a reversible adsorbing surface in voltammetry measurements. The model retains the essential features of modelling the adsorption system of interest whilst having a two dimensional geometry of the diffusion field which allows extensive simulation to explain all parameters which would be impossible for any three dimensional model. We show that the adsorption effect can have strong influence on the current value as well as the shape of the respond voltammogram, and is therefore generally important for studies using electro-active particles that can potentially be adsorbed on the surface surrounding the electrode.

Table 1: Illustrative examples of modified surfaces to providing preconcentration of the target analytes.

Publication	Modifying substrate	Target species
[5] Kaur & Srivastava, 2014	nanocrystalline metallosilicate	Riboflavin, Rutin, Pyrodoxine
[6] Yu et al. , 2013	Co_3O_4 nanocrystals	Pb(II)
[7] Zhang et al. , 2013	$\alpha - MnO_2$	Zn(II), Cd(II), Pb(II), Cu(II), Hg(II)
[8] Xu et al. , 2013	hollow nano-spheres of magnesium sillicate	Cd(II), Pb(II), Cu(II), Hg(II)
[9] Liu et al. , 2013	porous Co_3O_4 microsheets	Pb(II)
[10] Herzog et al. , 2013	mesoporous organosilica	Hg(II)
[13] Zhang et al. , 2011	nano-wall arrays of $CaCO_3$ chitosan	organophosphate pesticides
[11] Mbouguen et al. , 2011	bilayer of organoclay overcoating sublimed ferrocene layer	ascorbic acid, uric acid
[14] Zhang et al. , 2011	flower-like hydroxyapatite	Cd(II), Pb(II)
[12] Tonlé et al. , 2010	thiol-functionalized clay	Pb(II)
[15] Yin et al. , 2010	nano-'shuttles' of copper oxide (CuO)	Hg(II)

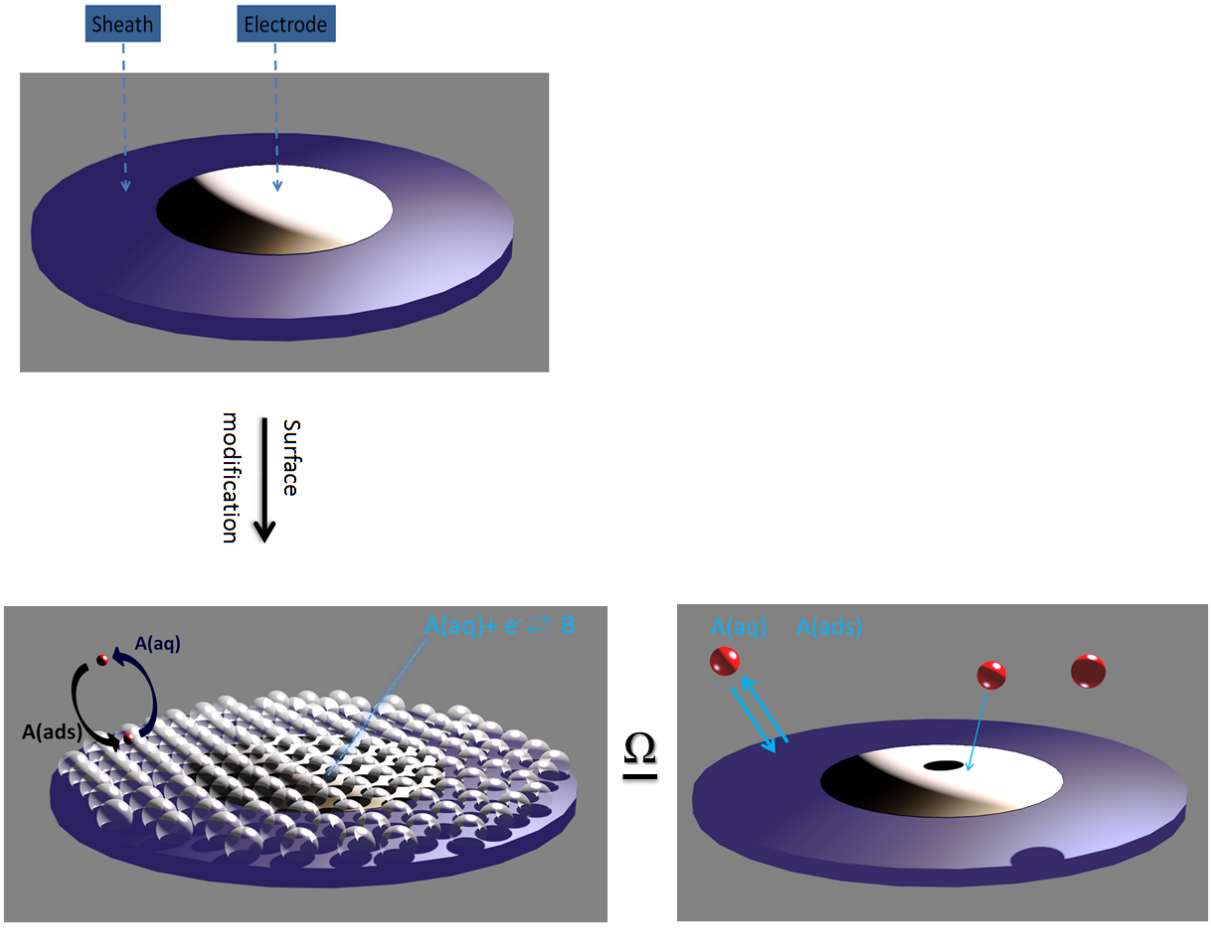

Figure 1: Illustration of the idealized model for the simulation of pre-concentrated specie A (red spheres) on the modifier (white spheres) around the electrode.

Theory

We consider a cyclic voltammetry simulation of a system contains small finite disc electrode surrounded by an insulating but adsorbing/desorbing sheath. The sheath is assumed to behave according to the reversible Langmuir model of surface adsorption.[22] This study is made via simulating Fickian diffusion under the presence of supporting electrolyte, allowing a diffusion controlled transport. By approximating the transport to behave in a statistical manner,[23–25] we can avoid complex stochastic modelling and solve numerically the Fick's second law in the solution.[26,27] For a finite disc geometry (figure 2a), we can solve Fick's second law for a redox couple in a cylindrical space using axial symmetry around $r = 0$:[28]

$$\begin{aligned} \frac{\partial c_A}{\partial t} &= D_A \left(\frac{\partial^2 c_A}{\partial r^2} + \frac{\partial^2 c_A}{\partial z^2} + \frac{1}{r}\frac{\partial c_A}{\partial r} \right) \\ \frac{\partial c_B}{\partial t} &= D_B \left(\frac{\partial^2 c_B}{\partial r^2} + \frac{\partial^2 c_B}{\partial z^2} + \frac{1}{r}\frac{\partial c_B}{\partial r} \right) \end{aligned} \tag{2}$$

where r and z are the cylindrical coordinates, D is the diffusion coefficient, c is the concentration, and the symbols A and B are the redox couple species in the one step one electron electrochemical reaction:

$$A \leftrightarrows B + e^- \tag{3}$$

We define two distances in the r direction, the disc electrode radius (r_d) and the surface radius (r_s) as illustrated in figure 2.

Dimensionless coordination representation

Dimensionless parameters are used in the simulation to simplify the analysis.[28] All the dimensional and dimensionless symbols presented in this work, are also summarized in Table 2. Coordinates are normalized to the surface radius ($R = r/r_s, Z = z/r_s$) and concentrations are defined relative to the bulk concentration of the electroactive species ($C = c/c^*$). The

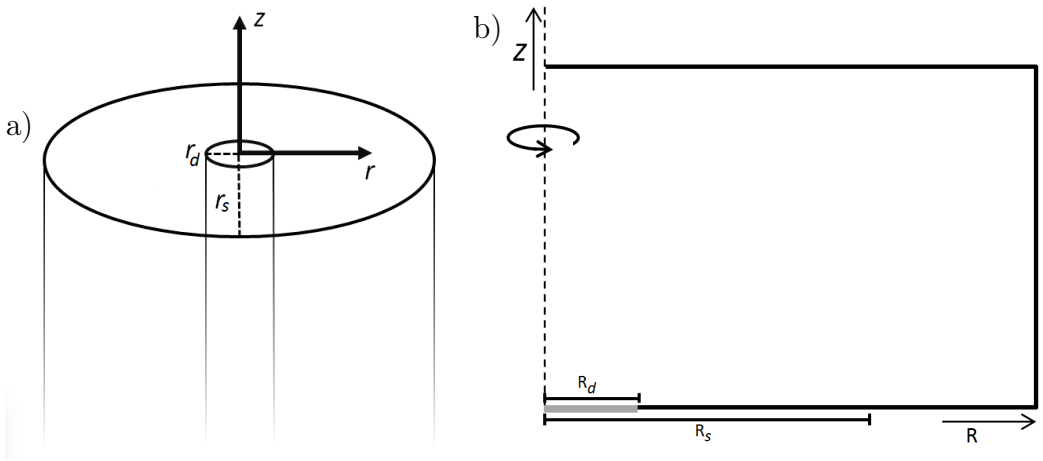

Figure 2: 3D Illustration of the microdisc electrode surrounded by a sheath (a) and the 2D dimensionless system in the simulation model (b).

diffusion coefficient of the product species (B) can be related to the diffusion coefficient of species A by:

$$d_B = D_B/D_A \tag{4}$$

Further, a dimensionless time parameter (τ) is defined as:

$$\tau = \frac{D_A}{r_s^2}t \tag{5}$$

In the transformed coordinates, the radius of the surface is unity and the microdisc electrode lies between: $0 < R_d < 1$. Converting Fick's second law into a dimensionless form gives:[29]

$$\begin{aligned} \frac{\partial C_A}{\partial \tau} &= \left(\frac{\partial^2 C_A}{\partial R^2} + \frac{\partial^2 C_A}{\partial Z^2} + \frac{1}{R}\frac{\partial C_A}{\partial R}\right) \\ \frac{\partial C_B}{\partial \tau} &= d_B\left(\frac{\partial^2 C_B}{\partial R^2} + \frac{\partial^2 C_B}{\partial Z^2} + \frac{1}{R}\frac{\partial C_B}{\partial R}\right) \end{aligned} \tag{6}$$

The dimensionless mass transport equations must be solved over all space with the appropriate boundary conditions which define the kinetics and fluxes on the surfaces; the disc and the sheath (figure 2b).

Table 2: Dimensional and dimensionless parameters

Parameter	Description	Units
Dimensional parameters		
A	Electrode area	cm^2
r_d	Electrode radius	cm
r_s	Surface radius	cm
D	Diffusion coefficient	$cm^2 s^{-1}$
c	Concentration	$mol\, cm^{-3}$
c^*	Bulk solution concentration	$mol\, cm^{-3}$
θ	Fractional surface coverage	
θ_{eq}	Initial coverage state	
Γ	Surface coverage of a full monolayer	$mol\, cm^{-2}$
k^0	Standard electrochemical rate constant	$cm\, s^{-1}$
k_0	Adsorption rate constant	$cm\, s^{-1}$
k_1	Desorption rate constant	$mol\, cm^{-2}\, s^{-1}$
t	Time	s
j^D	Flux	$mol\, cm^{-2}\, s^{-1}$
J^D	Rate	$mol\, s^{-1}$
α, β	Symmetry coefficients	
R	Gas constant	$J\, mole^{-1} K^{-1}$
E	Potential	V
E_f^0	Formal potential	V
Dimensionless parameters		
j	Dimensionless flux density	
J	Dimensionless net flux	
$C_{A,B}$	$c_{A,B}/c^*_{A,B}$	
R	r/r_s	
Z	z/r_s	
d_B	D_B/D_A	
τ	$D_A t/r_s^2$	
K^0_{BV}	$k^0 r_s/D_A$	
K_0	$k_0 r_s/D_A$	
K_1	$\frac{k_1 r_s}{D c^*_A}$	
γ	$\Gamma(\frac{1}{c^*_{A(r,0)^{r_s}}})$	
ϕ	F(E-E_f^0)/RT	
σ	Dimensionless scan rate, $r_s^2 \frac{F}{D_A RT}$	

Boundary conditions

At $z = 0$ we define the kinetics of the adsorbing surface ($R_d < R \leq R_s$), and the electrode boundary condition ($R \leq R_d$). At the disc electrode, the boundary condition is set to be the flux of each species correlated to the electrode potential (E) according to the Butler-Volmer equation:

$$\begin{array}{l} \tau \geq 0 \\ 0 < R \leq R_d \end{array} \qquad \left(\frac{\partial C_{A(R,0)}}{\partial Z}\right)_{Z=0} = K^0_{BV}\left(C_{A(R,0)}e^{-\alpha\phi(\tau)} - C_{B(R,0)}e^{\beta\phi(\tau)}\right) \tag{7}$$

K^0_{BV} is the dimensionless rate constant given by $k^0 r_s/D_A$ where k^0 is the standard heterogeneous rate. α and β are the symmetry parameters, and E^0_f is the formal potential. $\phi(\tau)$ is equals to $F(E - E^0_f)/RT$. The potential depends on the scan rate and time via:

$$\begin{aligned} Forward\,scan: &\quad E < E_{max} \quad E = t\nu + E_{min} \\ Backward\,scan: &\quad E > E_{min} \quad E = E_{max} - t\nu \end{aligned} \tag{8}$$

and in dimensionless form depends on the dimensionless scan rate ($d\phi/d\tau$) applied in a cyclic voltammetry measurement:

$$\begin{aligned} Forward\,scan: &\quad \phi < \phi_{max} \quad \phi(\tau) = \tau\sigma + \phi_{min} \\ Backward\,scan: &\quad \phi > \phi_{min} \quad \phi(\tau) = \phi_{max} - \tau\sigma \end{aligned} \tag{9}$$

σ is therefore the dimensionless scan rate , and $\phi_{min,max}$ are the lowest negative and highest positive dimensionless potentials in the cyclic voltammetry, respectively. In this study, ϕ_{min} set to -20 and ϕ_{max} to +20, far enough from the expected redox peaks. We also consider K_{BV} to be fast enough to simplify the model, and since its role is not in primary importance in this study.

Applying mass conservation of the electrochemical reaction, we can set the flux boundary

condition of species B to be:

$$\begin{matrix}\tau \geq 0 \\ 0 < R \leq R_d\end{matrix} \qquad \left(\frac{\partial C_A}{\partial Z}\right)_{Z=0} = -d_B \left(\frac{\partial C_B}{\partial Z}\right)_{Z=0} \tag{10}$$

We next consider the boundary condition for the adsorption of species on the sheath surface.[23,30] The process is described as a first order reversible reaction, according to the Langmuirian model.[22] Therefore, the dimensional flux of species A on the adsorbing surface is given by:

$$\begin{matrix}\tau > 0 \\ r_d < R \leq r_s\end{matrix} \qquad D_A \left(\frac{\partial c_A}{\partial z}\right)_{z=0} = k_0 \left(1-\theta\right) c_{A(r,0)} - k_1 \theta \tag{11}$$

where θ is the fractional coverage and varies between zero to unity. The adsorption and desorption rate constants are denoted by $k_0 (cm\, s^{-1})$ and $k_1 (mole\, cm^{-2} s^{-1})$, respectively. Converting k_0 and k_1 to dimensionless rate constants gives:

$$K_0 = \frac{k_0 r_s}{D_A},\ K_1 = \frac{k_1 r_s}{D_A c_A^*} \tag{12}$$

Following that we rewrite the flux equation in a dimensionless form to define the surface boundary condition:

$$\begin{matrix}\tau > 0 \\ R_d < R \leq R_s\end{matrix} \qquad \left(\frac{\partial C_A}{\partial Z}\right)_{Z=0} = K_0 \left(1-\theta\right) C_{A(R,0)} - K_1 \theta \tag{13}$$

$\Gamma\, (mole\, cm^{-2})$ is defined as the maximum coverage. Hence, the variation of θ with t can be denoted as:

$$\Gamma \frac{\partial \theta}{\partial t} = k_0 \left(1-\theta\right) c_{A(r,0)} - k_1 \theta \tag{14}$$

and in dimensionless form:

$$\gamma \frac{\partial \theta}{\partial \tau} = K_0 \left(1-\theta\right) C_{A(R,0)} - K_1 \theta \tag{15}$$

where γ is a dimensionless coverage. By combining Eq. 12 and Eq. 15, and substituting τ and C_A with $D_A t/r_s^2$ and c_A/c_A^*, respectively :

$$\gamma \frac{r_s^2}{D_A} \frac{\partial \theta}{\partial t} = \frac{k_0 r_s}{D_A} (1-\theta) \frac{c_{A(r,0)}}{c^*_{A(r,0)}} - \frac{k_1 r_s}{D_A c^*_{A(r,0)}} \theta \tag{16}$$

Rearranging,

$$c^*_{A(r,0)} r_s \gamma \frac{\partial \theta}{\partial t} = k_0 (1-\theta) c_{A(r,0)} - k_1 \theta \tag{17}$$

and by using Eq. 14 and Eq. 17 we obtain the dimensionless maximum coverage:

$$\gamma = \Gamma(\frac{1}{c^*_{A(r,0)} r_s}) \tag{18}$$

For species B, on the sheath surface ($R_d < R \leq R_s$) we define a wall boundary condition:

$$R_d < R \leq R_s \qquad \left(\frac{\partial C_B}{\partial Z}\right)_{Z=0} = 0 \tag{19}$$

It is important to note that it is reasonable to assume that only species A can adsorb/desorb since in the case where species B does adsorb, only a very small effect on the result is seen for the forward peak which is the basis of the sensing application described in the introduction. Moreover, since oxidation/reduction changes the charge on A it is likely that neutral A molecules would adsorb more than charged B molecules.

Beyond the adsorbing/desorbing surface, at $Z = 0$, we define a wall boundary condition for both species A and B:

$$R_s < R \leq R_{max} \qquad \left(\frac{\partial C_{A,B}}{\partial Z}\right)_{Z=0} = 0 \tag{20}$$

From symmetry, the flux across the Z axisymmetric boundary can be set to zero:

$$\left(\frac{\partial C_{A,B}}{\partial R}\right)_{R=0} = 0 \tag{21}$$

The edges in the outer space of the simulation set to the bulk concentration:

$$C_{R_{\max}} = 1, \quad C_{Z_{\max}} = 1 \tag{22}$$

where R_{max} and Z_{max} are set to be far enough from the root mean squared displacement according to the Einstein equation:[31,32]

$$\begin{aligned} R_{\max} &= 1 + 6\sqrt{\tau_{\max}} \\ Z_{\max} &= 6\sqrt{\tau_{\max}} \end{aligned} \tag{23}$$

and $\tau_{\max}$ is chosen to be a full time of one cycle in the CV:

$$\tau_{\max} = \frac{2(\phi_{max} - \phi_{min})}{\sigma} \tag{24}$$

Initial conditions

The initial dimensionless concentration of the electro-active species (C_A) is set to 1, and for the oxidized form (species B), the concentration is set to 0. It is assumed that before caring out the cyclic voltammetry measurement, the surface of the sheath adsorbs particles until an equilibrium on the surface is achieved before applying potential. Therefore, rearranging eq. 13 where C equals to 1 and the flux equals to 0, gives the initial coverage of the adsorbing/desorbing surface of the sheath in equilibrium state corresponding to the familiar Langmuir isotherm:

$$\begin{aligned} &\tau = 0 \\ &R_d < R \leq R_s \end{aligned} \qquad \theta_{eq} = \frac{K_0}{K_0 + K_1} \tag{25}$$

Current calculation

The dimensionless flux inward the disk electrode is given by:

$$\begin{aligned} disk: \quad & 0 < R \leq R_d \\ surface: \quad & R_d < R \leq R_s \end{aligned} \qquad j = \left(\frac{\partial C_A}{\partial Z}\right)_{Z=0} \tag{26}$$

By integrating the flux (j^D) over the disc and the surface, we can obtain the net flux(J^D) inward the disc electrode and the adsorbing/desorbing flux on the surface surrounding it:

$$J_d^D = 2\pi \int_0^{r_d} j_{r,0}^D r \mathrm{d}r \,, \quad J_s^D = 2\pi \int_{r_d}^{r_s} j_{r,0}^D r \mathrm{d}r \tag{27}$$

In dimensionless form we get:

$$J_d = 2\pi \int_0^{R_d} j_{R,0} R \mathrm{d}R \,, \quad J_s = 2\pi \int_{R_d}^{R_s} j_{R,0} R \mathrm{d}R \tag{28}$$

Assuming a single electron transfer, the dimensional Faradaic current inward the microdisc electrode is obtained as follows:

$$I_d = 2\pi F c_A^* D r_s \int_0^{R_d} j_{R,0} R \mathrm{d}R = F J_d^D \tag{29}$$

Numerical methods

The partial differential equations for both species, along with the boundary conditions are solved numerically with the finite difference method for each time step, using the implicit Crank-Nicolson method.[33] These equations are discritized over an expanding spatial 2D grid with m_{max} rows and n_{max} columns ($R(n_{max}) \times Z(m_{max})$). This space is meshed with an expanding grid around 3 nodes: $\delta R, R_d, R_s$, where a large perturbation of flux is expected. The first differences around the nodes are set to be with the minimum δR and δZ values,

after which the differences grow exponentially to cover all the space as follows:

$$
\begin{aligned}
&R\ grid: \\
&R_{n+1} = R_n \rho_R \qquad \delta R < R_n < \tfrac{R_d}{2},\ \ R_d < R_n < \tfrac{R_s+R_d}{2},\ \ R_s < R_n < R_{max} \\
&R_{n+1} = R_n / \rho_R \qquad \tfrac{R_d}{2} < R_n < R_d,\ \ \tfrac{R_s+R_d}{2} < R_n < R_s \\
&Z\ grid: \\
&Z_{m+1} = Z_m \rho_Z \qquad 0 < Z_m < Z_{max}
\end{aligned}
\tag{30}
$$

where ρ_R and ρ_Z are the expansion factors between two adjacent cells in the rows R_{n+1} to R_n and in the columns Z_{n+1} to Z_n, respectively . The concentration equations is set to each specie (A and B) in the space.

Using the alternating direction implicit (ADI) method, we can solve the 2D mass transport system in parallel computing. Each individual direction (R_n, Z_m) in the ADI method is solved for the two species. This allows the solution of the finite difference equations in a form of tri-diagonal matrices to be obtained in $O(2 \cdot m_{max} \cdot n_{max})$ operations at each time step. In the Z directions where species A is coupled with species B (on the electrode boundary), we define one tri-diagonal matrix to solve the set of concentration equations for both species[34] .

Numerical convergence achieved with the following values: $\delta R = 1 \times 10^{-5}, \delta Z = 1 \times 10^{-8}$ (the minimal differences next to the nodes), and $\rho_R = 1.15, \rho_Z = 1.15$ (the expanding factors of the grid) ensuring that the calculations are sufficiently accurate at a practicable solving time. It is important to minimize δZ relative to $\tau_{max} \times (\theta/\Gamma)$ in order to avoid numerical error accumulation in the coverage. As will be mentioned also in the result section, in cases of very fast coverage changes $(d\theta/d\tau)$, the numerical parameters chosen for the simulation are insufficient for achieving a smooth cyclic voltammetry (CV), or even not applicable. Hence in order to stay in practical calculation time and real systems zone, we limited the upper range of K_0 and K_1 to a maximum value of 10,000.

Simulations were coded in C++ with the OpenMP(Open Multi-programming) API for parallel programming. The simulations preformed on an Intel (R) Xeon (R) 3.2Ghz, with

approximately usage of 0.5GB RAM, and runtime between of 20 minutes for each CV calculation.

Results and discussion

We first discuss a representative case where a reversible adsorption/desorption occurs on the surface of the supporting sheath under typical practical conditions of cyclic voltammetry. This introduces the basic physical effects on the voltammetry and discusses the main roles of a reversible surface in the CV measurement. Following that, we present a parametric study, where we present the trends in the voltammetry that depend on various important physical parameters.

It is worth to mention that all CVs start assuming a fully equilibrated state of the adsorbing/desorbing surface with the solution. This would likely be also the case in mostly all the electro-analytical systems mentioned, except if the particles of interest are not present in the system before the applying of the potential.[35]

Cyclic voltammetry with a reversible adsorbing sheath - a representative case

We first carried out a simulation to describe the effect of the reversible adsorbing/desorbing surface of the sheath ('active surface'), using the following parameters $K_{eq}(K_0/K_1) = 0.1$ and $K_0 = 10$. A radius ratio of $1 : 10(R_d/R_s)$ was used. The surface maximum density γ was chosen to be 100. In practice, typical values for $D(10^{-9}m^2\,s^{-1}), c(1mM)$, and $r_s(10\mu m)$, would give k_0 and k_1 to be $10^{-2}m\,s^{-1}$ and $10^{-3}mole\,s^{-1}\,m^{-2}$, respectively, and this corresponds to realistic values of $\Gamma = 10^{-9}mole\,cm^{-2}$. The dimensionless scan rate of the CV set to an intermediate value of ($\sigma = 10$), so other effects of interest, as from the supporting sheath's surface can be clearly captured. For comparison, we also ran a 'blank CV' simulation for a disc with the same conditions, only without any adsorption/desorption ('non-active surface') , K_0 and K_1 were equal to zero.

Figure 3 presents the voltammograms for both cases. In the 'non-active surface' , the CV shows the expected behaviour of the current response in a disc electrode. Since the scan rate

is intermediate, a small peak is observed and shifts the voltammogram from true steady state behaviour, towards a partial transient behaviour. It is also observed that the normalized current approaches the steady state value, 1, as in the case of a finite disc ($4nFDC^*R$).[36] However, under the condition of an 'active surface', we observe a large oxidation peak that evolves during the forward scan, whilst the reduction peak remains almost unchanged. The oxidation peak is clearly a result of large extra amount of species A that can be released from the surface and flow towards the disc electrode, in the zone of the diffusion layer, where the concentration of species A is otherwise more depleted. The back reduction peak is not strongly influenced by the 'active surface' as observed from figure 3, since species B is assumed to not have an interaction with the surface of the sheath.

A "snapshot" of the concentration maps for the two cases were taken in the forward scan at the dimensionless potential of 2.0, slightly before the peak gets to full hight. These maps are presented in figure 4a. A difference concentration map is also provided in figure 4b to emphasis the concentration changes between the two cases. In comparison between the 'non-active surface' and the 'active surface', it is seen that the diffusion layer in the R direction is significantly narrower for the case of an active adsorbing/desorbing surface. For the 'non-active surface', the radial diffusion layer has a normal shape and is expanded in the same manner along the R and Z directions, while in the case of the 'active surface', as desorption occurs, a compensation of accessible material that is released from the supporting surface creates a sharper and narrower gradient in the R direction, and therefore alters the oxidation current measured in the CV.

Another way to understand the role of the surface is to examine the change in the coverage on the surface. Figure 5 shows coverage as a function of potential at R=0.1 and 1.0 and reveals that most of the contribution of the current is via desorption from the inner side of the surface close to the disc. The area far from the disc shows only small change in the coverage along the CV. Since we describe the sheath with the Langmuir model, it can be seen that when the coverage gets to low values with increasing ϕ, the desorption becomes moderated,

and as a consequence, the compensation of access material towards the disc becomes limited for the high potentials, thus resulting in a peak shape at the CV as was observed in figure 3.

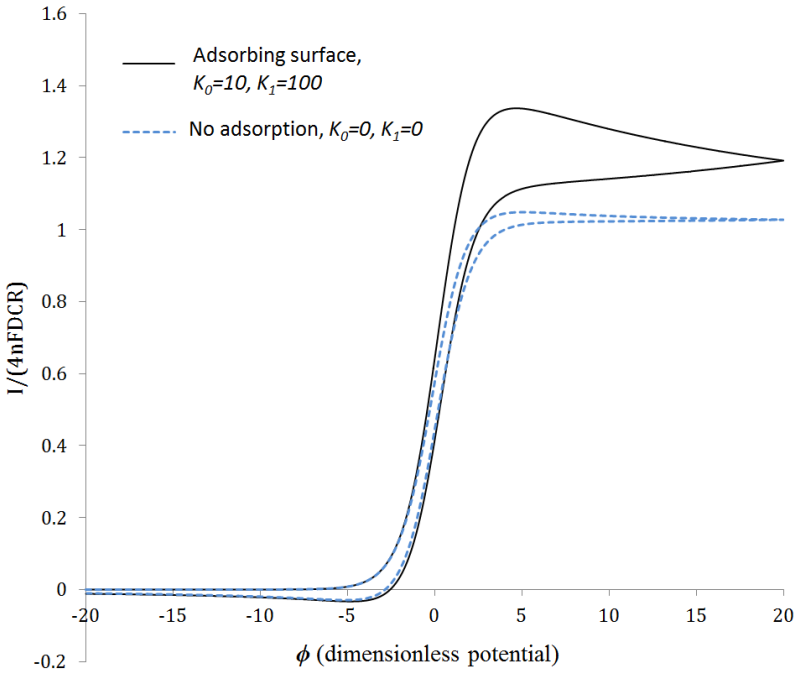

Figure 3: Cyclic voltammetry at a non-adsorbing surface (dashed curve), and cyclic voltammetry in a reversible case(solid curve). Other conditions: $\sigma = 10$, $R_s/R_d = 10$, $D_A = D_B = 1$.

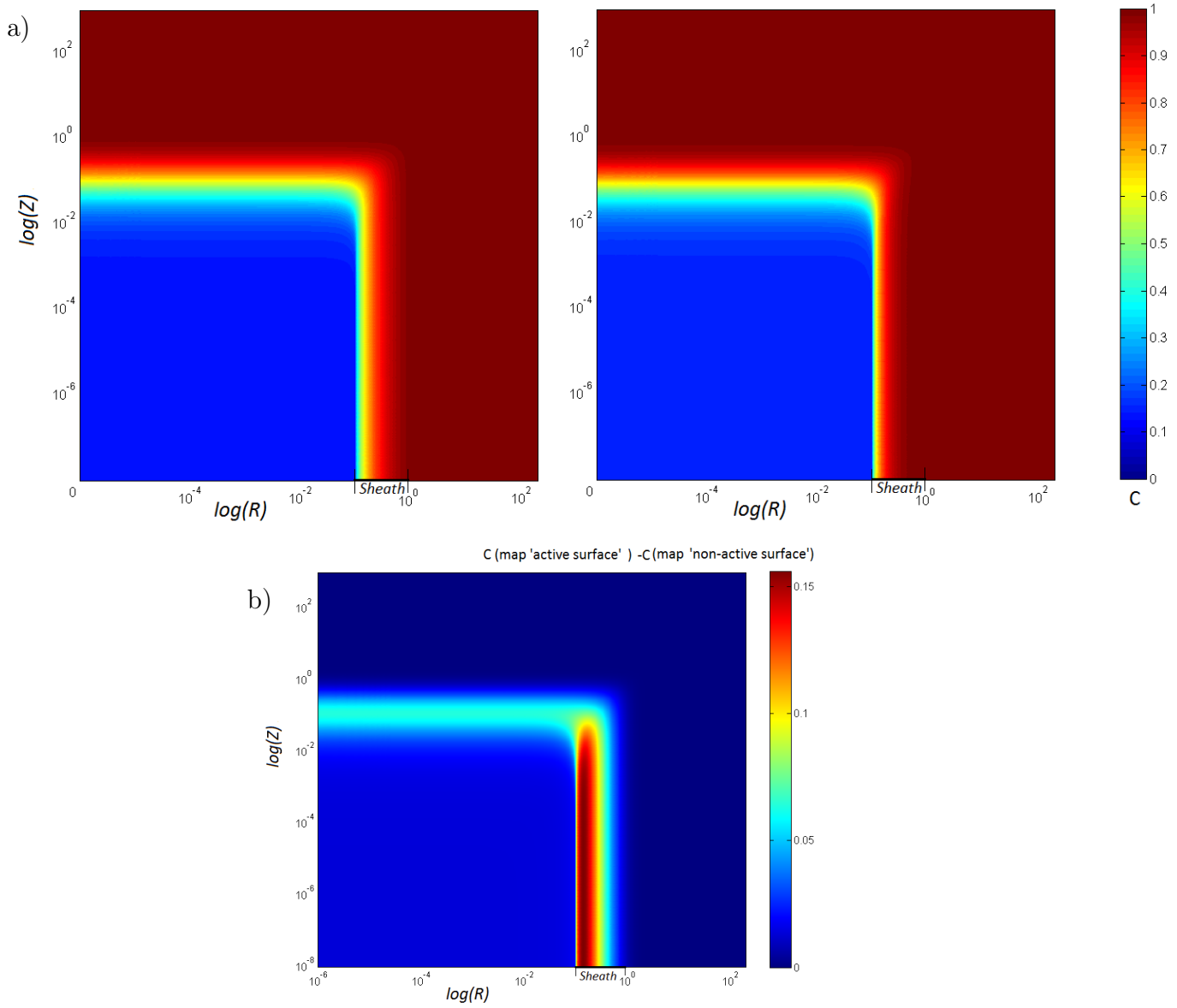

Figure 4: a) Concentration maps in logarithmic scaled space, at $\phi = 2.0$ in the forward scan. The left colour map is with a non-active surface, the right colour map is for 'active surface' where: $K_1 = 100$ and $K_0 = 10$. b) difference concentration maps between the absolute concentration values of the 'active surface' map and the 'non-active surface' map. Other conditions: $\sigma = 10$, $R_s/R_d = 10$, $D_A = D_B = 1$.

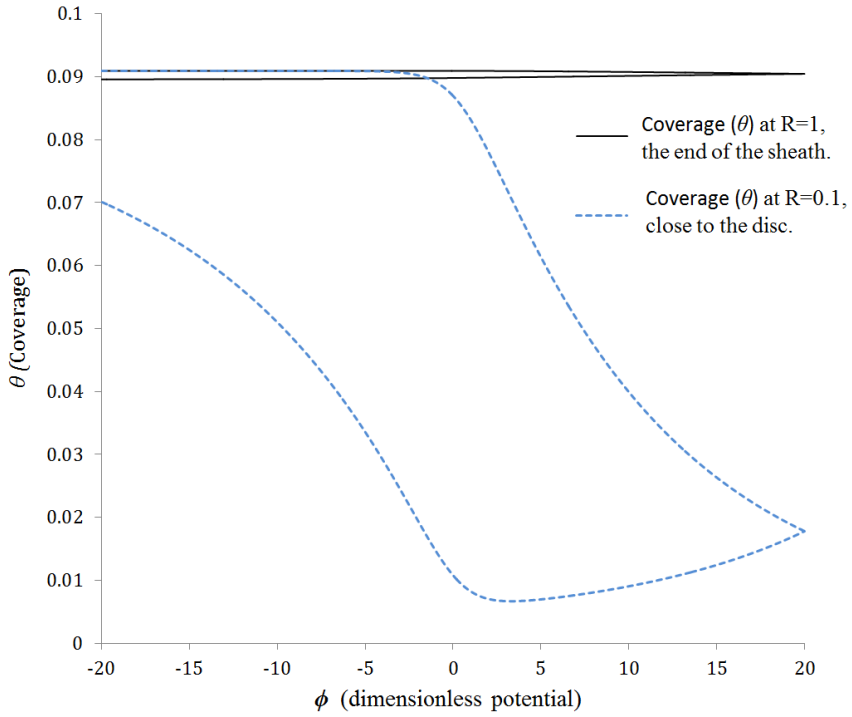

Figure 5: Coverage (θ) profiles in the reversible adsorbing/desorbing surface along the cyclic voltammetry. The dashed curve stands for the beginning of the sheath closest to the disc ($R = 0.1(R_d)$). The solid line shows the coverage in the end of the sheath at $R = 1(R_s)$. Other conditions: $\sigma = 10$, $R_s/R_d = 10$, $D_A = D_B = 1$.

From the results for this representative case, we report that a reversible adsorbing sheath, not only can increase the current response significantly, but also may alter the shape of the voltammogram from steady state to transient 'peak like' shape. These effects on the current values and the shape, are controlled by the sheath properties and also by the voltammetry parameters, as we next discuss.

Parametric study

In order to understand the influence of the adsorbing/desorbing surface properties on the CV measurements, we next carried out series of CV simulations changing the sheath parameters: K_0, K_1, γ, and R_{sd}.

Adsorption / desorption rates

In this study, we demonstrate how the CV is effected due to the change of the surface rate constants, K_0 and K_1. We use the same values for $\gamma = 100$,$\sigma = 10$, and the same radius ratio ($R_s/R_d = 10$) as in the previous section. Figure 6 shows the voltammograms for variable K_1 and constant K_0 (figure 6a), and for constant K_1 and variable K_0 (figure 6b).

In figure 6a, it is shown that the oxidation current is altered significantly as the desorbing rate increases. However, at a high rate of K_1 and relative low rate of K_0 ($K_0 = 100, K_1 = 1000$, figure 6a), the current decreases. This is explained as follows; due to the fast rate of desorption and low initial coverage (θ_{eq}) the surface of the sheath is drastically diluted within the time scale of the CV at this particular scan rate, leading to insufficient available material for desorption before fully exploiting the diffusion transport towards the disc electrode. Subsequently, it results in a significant relaxation of the current and also a clear transient oxidation peak.

Moreover, figure 6b shows that increasing K_0 also alters the oxidation current. The starting point of the measurement corresponds to an equilibrium coverage (θ_{eq}), and therefore faster K_0 results in higher θ_{eq}. Consequently, the surface has larger amount of material, accessible for desorption, during the CV. However, in the highest presented value of $K_0 = 1000$ and $K_1 = 100$, the current decreases. This means that the adsorption term in equation 13, $K_0\,(1-\theta)\,C_{A(R,0)}$ becomes more dominant, and it implies that faster mass transport (higher scan rate) can reduce back this term and alter the current for this kinetic rates. In effect there is stronger adsorption on the surface.

It is important to mention that at extremely high rates, the simulated voltammograms

become "noisy" due to large changes in the coverage along the adsorbing sheath relative to the spacing of the simulation mesh. The noise can be reduced by significantly reducing the values of ρ_R and ρ_Z. However, for larger rates it becomes impossible to have a fully smooth simulation unless $\delta\tau$ is decreased significantly (by orders of magnitudes), which would make the calculation impracticable even for significant powerful computers. This instability is also inversely proportional in γ and thus when higher γ is applied, larger kinetic rates can be investigated for these numerical calculations.

It can be seen from figure 6, that the CV measurement not only depends on the surface rate constants K_0 and K_1 independently, but also with their ratio, $K_{eq} = K_0/K_1$. In order to clarify more this dependency, we performed a set of simulations, scanning K_0, K_1 in the range between 10^{-4} to 10^4. The peak of each voltammogram was mapped into a surface plot presented in figure 7. In this way we can get a complete picture of the effect of the surface rates and thermodynamics on the maximum oxidation peak. The surface map shows that when K_0 is in the same order of K_1, the oxidation peak gives higher values. The maximum current is not exactly when $K_{eq} = 1$, but varies in the range of $K_0/K_1 = 1.5 - 3$; the surface map is not fully symmetric. The implication of these observations for practical analysis using adsorptive pre-concentration is firstly that the optimum surface requires a delicate balance of kinetics and thermodynamics that is likely to be beyond rational prediction, implying the essential need for empiricism in this area. Secondly, the maximum change of current is less than an order of magnitude implying that pre-concentration via surface adsorption has limited analytical value. In principle, only optimizing *all* the following parameters; K_1, K_0 and γ results in further significant enhancement of the current, but order of magnitude is unlikely for practical situations.

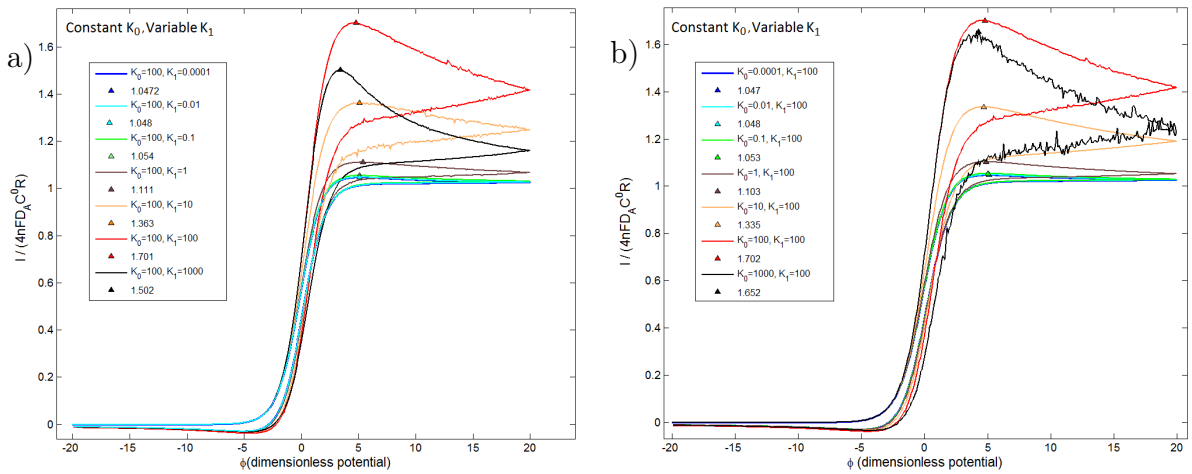

Figure 6: Voltammograms for constant K_1 and variable K_0 (a) and voltammograms for variable K_1 and constant K_0 (b), under the conditions: $\sigma = 10$, $\gamma = 100$, $R_s/R_d = 10$, and $D_A = D_B = 1$.

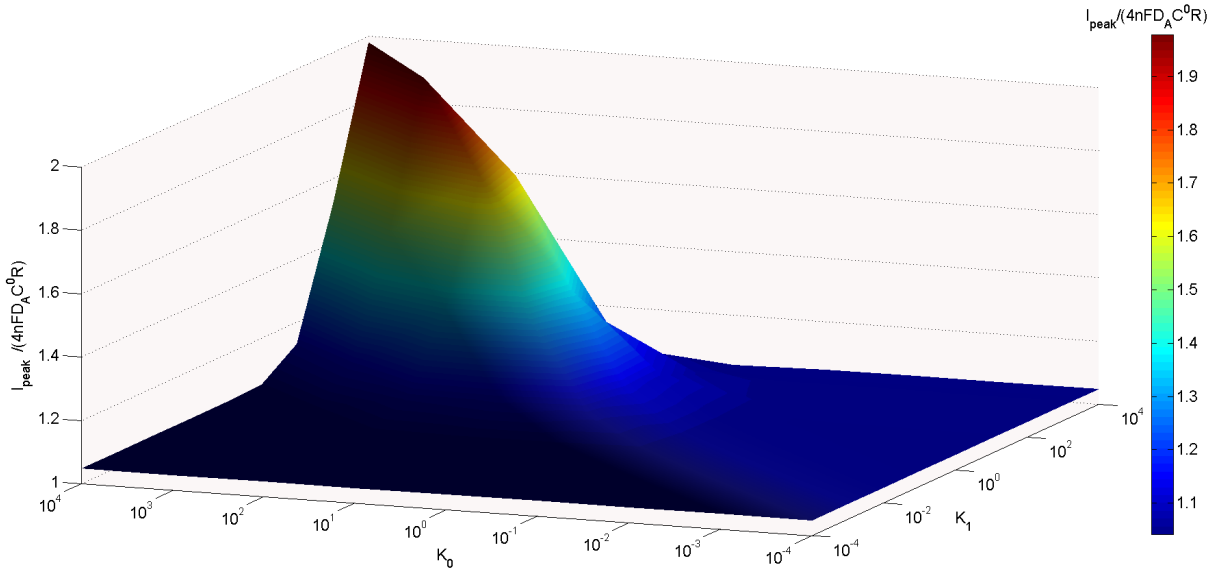

Figure 7: Surface map of the oxidation peak in a set of CV simulations, when K_1 and K_2 are scanned between 10^{-4} to 10^4. The map consists 9x9 matrix of the oxidation peaks. The CVs were carried out in the following conditions: $\sigma = 10$, $\gamma = 100$, $R_s/R_d = 10$, and $D_A = D_B = 1$.

Maximum surface coverage(γ)

The maximum surface coverage is an essential parameter for predicting the effect of desorption on the CV measurement. Figure 8 presents the voltammograms at various γ and figure 9 shows the coverage on the sheath near the disc electrode at $R = 1 + \delta R$.

It is shown in figure 8 that when γ gets to large values, the oxidation current increases significantly, due to the high amount of species A on the surface that is available for desorption. Nevertheless we can see that the reduction peak is not influenced by γ. Furthermore, it is observed that the voltammogram shape varies from transient behaviour with a clear peak to a steady state plateau (8). This can be explained by looking at the coverage changes in figure 9. At large γ, the coverage (θ) is only slightly changed during the CV, whilst for low γ, the contribution of flux towards the disc becomes limited after achieving low coverage during the forward scan.

It can be inferred from comparison between these figures (8, 9) that when the coverage remains unchanged during the CV, as in the case of $\gamma = 10^7$, the voltammograms have a steady state shape in the forward potential scan. Figure8 also shows that when γ reaches high values the current approaches a finite value. This is because θ remains: $K_0/(K_0 + K_1)$ for all τ, and therefore, the maximum flux from the surface in the case of high γ, is limited to :

$$J_s = -\frac{(1 - C_{R,0})K_0K_1}{K_0 + K_1}, \quad for\ all\ \tau\ where\ \ \gamma \longrightarrow \infty. \tag{31}$$

For lower values of $\gamma = 10^2, 10^5$, a gradual decreasing of the coverage occurs during the CV (figure 9), and the oxidation current is also characterized with a gradual drop (figure 8). In the cases of drastic and non linear drops of the coverage, an oxidation peak evolves ($\gamma = 10, 5, 2$). These results imply that the surface should be relatively accessible for adsorption sites in order to have a significant effect. At $\gamma = 10^{-2}$ or below, the influence of the surface is negligible, and the voltammetry has the same behaviour of a 'non-active surface'.

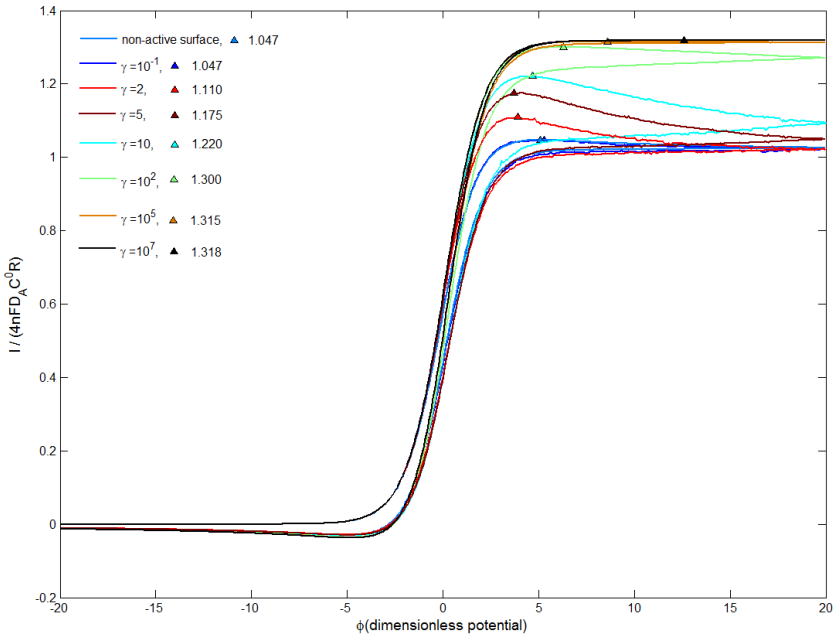

Figure 8: A comparison of voltammograms (coloured solid line, —) in various maximum surface adsorbing density (γ) and their oxidation peaks (coloured triangle, ▲). The CV simulations were carried out under the following conditions: $\sigma = 10$, $K_0 = 10$, $K_1 = 10$, $R_s/R_d = 10$, and $D_A = D_B = 1$.

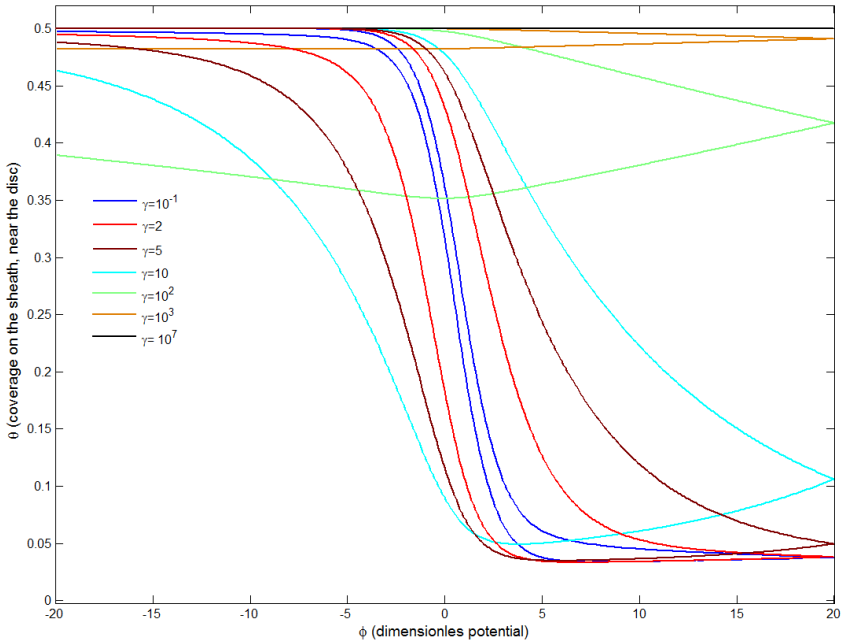

Figure 9: A comparison of the coverage during the CV simulations on the sheath, near the disc ($R = 1 + \delta R$). The comparison shows the coverage at various maximum surface adsorbing density (γ) in the range of $\gamma = 10^{-1}$ to 10^7). The CV simulations were carried out under the following conditions: $\sigma = 10$, $K_0 = 10$, $K_1 = 10$, $R_s/R_d = 10$, and $D_A = D_B = 1$.

Radius ratio (R_s/R_d)

We next consider a physical parameter, the radius of the sheath. In the model we described earlier, the sheath is described as the modifier in which analytes A can adsorb or desorb. The sheath size varies a lot for various electrochemical systems comprising micro and sub-micro disc electrodes, and can be in the range of less than one micrometre to an order of a millimetre. Here, in dimensionless system, the sheath size is reflected through the ratio of R_s/R_d. Therefore, we carried out cyclic voltammetry (CV) simulations in various ratios and present the influence of the sheath radius size on the CV measurement, in the case of reversible adsorption on the surface. In terms of using the disc/sheath geometry as a model for modified electrodes the study reflects the effect of changing the amount of modifier. Figure 10 shows the voltammograms at various radius ratio (R_s/R_d), for representative simulations made at $K_1 = 100$ and $K_0 = 10$. γ is chosen to be 100, and $\sigma = 10$. It is observed that for ratios above 5, the voltammetry does not change. This is due to the fact that far from the electrode the concentration gets close to the bulk concentration, and therefore little desorption flux occurs. This can also be studied from the coverage examination shown previously at figure 5. It was shown that the coverage at $R = R_s$ for the simulation of $R_s/R_d = 10$ remains almost unchanged during the CV. An interesting observation is that even at $R_s/R_d = 1.1$ a reasonable alteration of the oxidation peak is still seen (figure 10). It implies that even a 100nm coat surrounding a microdisc electrode can cause a significant effect on the current response in CV measurements. At the same time the implication for modified electrodes is that the benefits of modifing layers are confined to the case of relatively thin coats; the value of increasing the film thickness becomes progressively less with increasing size.

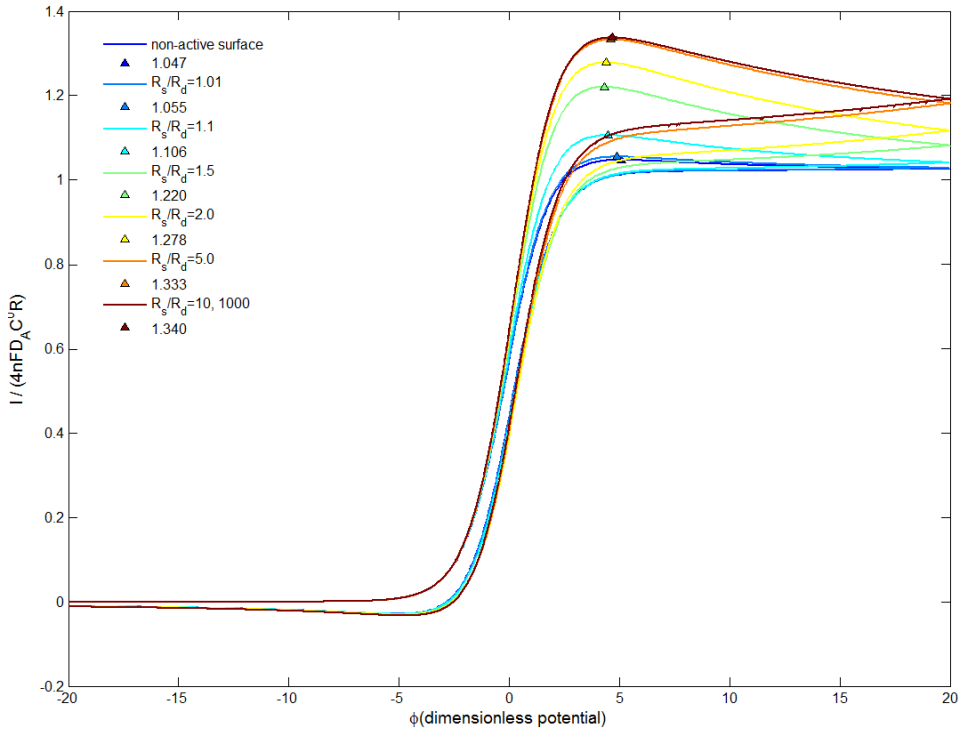

Figure 10: A comparison of the coverage during the CV simulations on the sheath, near the disc ($R = 1 + \delta R$). The comparison shows the coverage at various maximum surface adsorbing density (γ) in the range of $\gamma = 10^{-1}$ to 10^{7}). The CV simulations were carried out under the following conditions: $\sigma = 10$, $K_0 = K_1 = 10$, and $D_A = D_B = 1$.

Scan rate (σ)

Lastly, we chose to consider the scan rate parameter σ , since it can change dramatically the behaviour of the voltammetry. By changing the scan rate, two dominant physical properties reflect the surface response in the CV measurement of the disc electrode . The first is the mass transport that changes the concentration distribution around the disc as discussed earlier. The second is the time duration requires to scan the voltammogram. That said, when increasing the scan rate and reducing the time scale, a fast desorption for the surface can operate without reaching a low coverage that could limit the desorption.

The observations can be studied by examining two different scan rates for particular adsorbing/desorbing rate constants. Figure 11 compares CVs in $\sigma = 10$ (figure 11a) $\sigma = 100$ (figure 11b) of a 'non-active surface' and an 'active surface', where K_0, K_1 equals to 100 and 1000 (figure 11a summarizes certain voltammograms showed previously in figure 6) . Additionally, concentration profiles for species A in both scan rates, as well as extreme cases of fast scan rate ($\sigma = 625$) and very slow scan rate ($\sigma = 0.2$) , along Z=0 around the potential of oxidation and reduction peaks are provided in figure 12.

The result in figure 11 for the case where $K_0, K_1 = 100$ clearly shows that higher scan rate results in a greater compensation of species A flux from the adsorbing surface and alteration of the current significantly. The concentration profiles of the forward scan at figure 12 imply again that only the very close sites to the electrode are the dominant, since, even-though the averaged concentration along the surface is higher relative to the case of slower mass transport (broader diffusion layer), the greater concentration gradient close to the disc causes a larger alteration of the current via desorption of A species from the inner side of the surface. It can bee seen that the concentration profiles of the very fast and slow scan rates also follow the this trend.

It was shown above that for $\sigma = 10$, when K_0 or K_1 are increased from 100 to 1000 the current is reduced, since in this case, the surface coverage gets to very low values that limits the desorption from the surface towards the electrode. However, when increasing the scan

rate from 10 to 100 figure 11b, the surface does not reach the limitation of low coverage in the shorter time scale. As a consequence, the peaks get to higher values when K_0 or K_1 are increased from 100 to 1000, and the relaxation of the current following the peak is moderated in compare to the case of the lower scan rate ($\sigma = 10$).

The results also show that at $\sigma = 100$ and $K_0 = 1000$ or $K_1 = 1000$ the reduction peak is increased. From examining the concentration profiles of the backward peaks of both scan rates, it suggests that in the reverse scan, a significant higher concentration values of species A are observed in the solution adjacent to the disc for faster scan rates. These high values arise from the large desorption occurring during the CV, leading to the concentration of species A even in excess of the initial concentration (12). The latter shifts the reversible electrochemical reaction further to the reduction side. It is worth mentioning, that from examination of the concentration profiles of the extreme cases (very fast and slow scan rates) at $R = 0.1$, we can see the importance of choosing very small finite differences (δR) at the edge of the electrode to obtain stable calculations in very large concentration gradients.

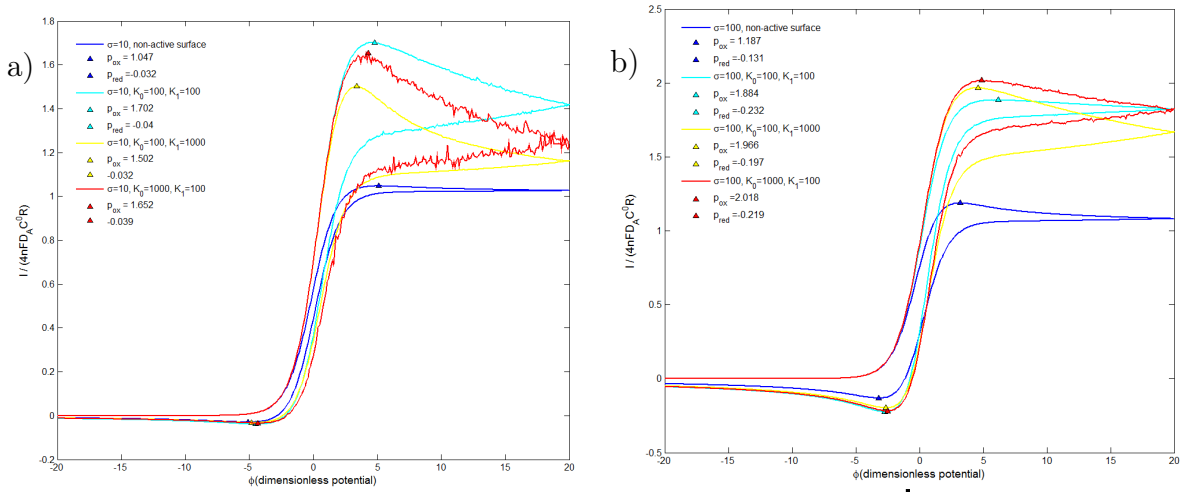

Figure 11: Comparison of two scan rates in CV Measurement on disc electrode surrounded by a reversible adsorption surface. (a) Voltammograms at $\sigma = 10$ and various K_1 and K_0. (b) Voltammograms at $\sigma = 100$ and various K_1 and K_0. $\gamma = 100$ for both (a) and (b). Other conditions: $R_s/R_d = 10$, $D_A = D_B = 1$.

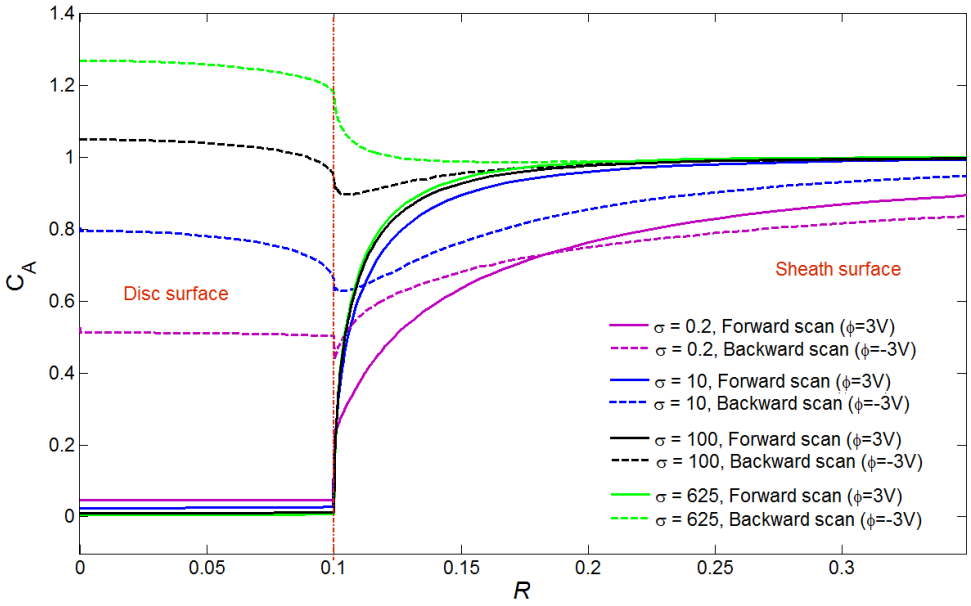

Figure 12: Concentration profiles of specie A on Z=0, at $\sigma = 10$ (blue lines) and $\sigma = 100$ (black lines), and also on extreme cases of $\sigma = 0.2$ and $\sigma = 625$. The profiles were taken in the forward oxidation peaks (solid lines) and backward reduction peaks (dashed lines). The CV simulations were carried out under the following conditions: $K_0 = 100$ and $K_1 = 100$, $\gamma = 100$. Other conditions: $R_s/R_d = 10$, $D_A = D_B = 1$.

Finally, we can generalize the influence of the scan rate on the voltammogram in a system with a disc surrounding a reversible adsorbing surface. Figure 13 shows CVs of an 'active-surface' and 'non-active surface' over a range of scan rates ($\sigma = 0.2 - 625$). The results show different stages of the voltammogram shape that evolves when changing the scan rate with an 'active surface' . At very low scan rate (figure 13a), the effect of the surrounding surface on the voltammogram is negligible due to the slow mass transport towards the disc electrode. Increasing the scan rate to an intermediate values (figure 13b-c) causes a peak, due to desorption of species A from the 'active surface'. This is in contrast to the steady state shape expected from the voltammetry on a microdisc electrodes. Further increase of the scan rates (figure 13d-e) results in another alteration of the voltammogram; in the case of an 'active surface' this stage is characterised by a significant increasing of the current and the voltammogram shape transforms to a steady state behaviour, as oppose to a transient behaviour observed in the 'non active surface'. This is due to the domination of the fast desorption of species A towards the disc electrode. At high scan rate (figure 13f), the desorption from the surrounding surface at these constant rates, is limited by the very fast mass transport occurs on the disc, and the transient behaviour of the voltammogram starts to evolve and then dominate the shape of the voltammogram.

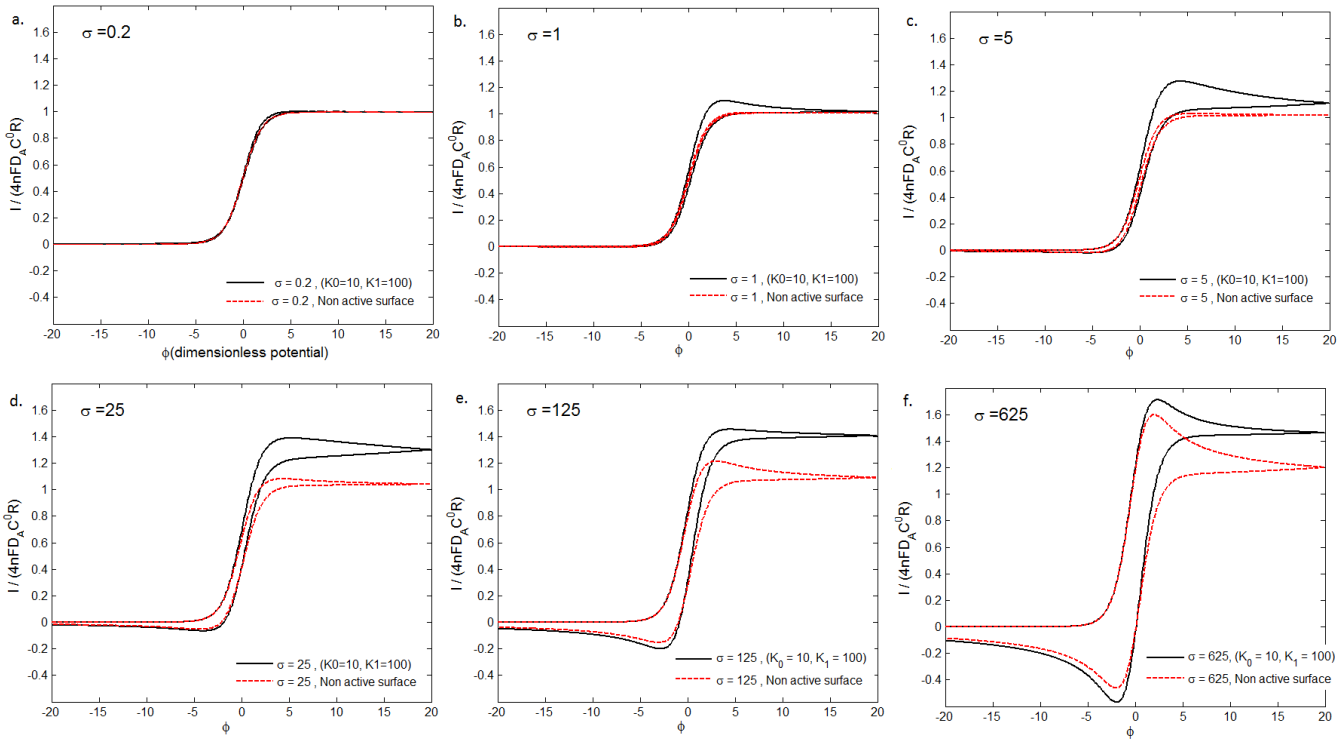

Figure 13: CVs of an 'active-surface'(black curves) and 'non-active surface' (red curves) in a range of scan rates: (a) $\sigma = 0.2$, (b) $\sigma = 1$,(c) $\sigma = 5$,(d) $\sigma = 25$, (e) $\sigma = 125$, (f) $\sigma = 625$. The CV simulations for the 'active surface' were carried out under the following conditions: $K_0 = 10$ and $K_1 = 100$, $\gamma = 100$. Other conditions: $R_s/R_d = 10$, $D_A = D_B = 1$.

Conclusions

We have shown that an adsorbing surface adjacent to the disc electrode can provide an enhancement of the voltammetry signal. This may be useful analytically but the current enhancements are limited because of the need for the both high surface coverage *and* fast desorption kinetics. It was specifically observed that desorption to adsorption rate ratio (K_{eq}) should be close to unity in order to achieve maximum enhancement of the signal.

The results shows that only the close sites to the electrodes dominate the surface response, and thus it implies that even a very thin coat of disc electrode can strongly effect the measurement. It can be suggested that in modified electrode surfaces, as discussed earlier in figure 1, the most important sites are those near the edge of the disc electrode where the current density is much higher due to the edge effect of transport towards finite disc. Equally the benefits of greatly increasing the thickness of modifying layers becomes progressively less the greater the thickness, tending to zero for thick coats.

Finally, the scan rate parameter was shown to have a dramatic influence on the behaviour of the adsorbing surface, and the voltammetry shape can vary from transient to steady state shape in dependence on the surface kinetics and coverage. The easy variation of the scan rate parameter in experimental systems can therefore give information about the kinetics of the surface and the ability to achieve efficient signal enhancement.

Acknowledgement

S. Eloul and R.G. Compton acknowledge funding from the European Union's Seventh Framework Programme (FP/2007-2013)/ERC Grant Agreement no. [320403].

S. Eloul is also supported by the Edward Penley Abraham Research fund, and the Chemistry Department of Oxford University.

References

(1) Ranganathan, S.; Guo, R.; Murray, R. W. Nanoparticle Films as Electrodes: Voltammetric Sensitivity to the Nanoparticle Energy Gap. *Langmuir* **2007**, *23*, 7372–7377.

(2) Richardson, J. N.; Peck, S. R.; Curtin, L. S.; Tender, L. M.; Terrill, R. H.; Carter, M. T.; Murray, R. W.; Rowe, G. K.; Creager, S. E. Electron-Transfer Kinetics of Self-Assembled Ferrocene Octanethiol Monolayers on Gold and Silver Electrodes from 115 to 170 K. *J. Phys. Chem-US* **1995**, *99*, 766–772.

(3) Chen, S. Nanoparticle Assemblies:Rectified Quantized Charging in Aqueous Media. *J. Am. Chem. Soc.* **2000**, *122*, 7420–7421.

(4) Murray, R. W. Nanoelectrochemistry: Metal Nanoparticles, Nanoelectrodes, and Nanopores. *Chem. Rev.* **2008**, *108*, 2688–2720, PMID: 18558753.

(5) Kaur, B.; Srivastava, R. Nanocrystalline Metallosilicate Modified Electrodes for the Simultaneous, Sensitive, and Selective Determination of Riboflavin, Rutin, and Pyridoxine. *Electroanal* **2014**, *26*, 1078–1089.

(6) Yu, X.-Y.; Meng, Q.-Q.; Luo, T.-J.; Yong-Sun, B.; Li, Q.-X.; Liu, J.-H.; Huang, X.-J. Facet-dependent electrochemical properties of Co_3O_4 nanocrystals toward heavy metal ions. *Sci. Rep.* **2013**, *3*, 1–7.

(7) Zhang, Q.-X.; Peng, D.; Huang, X.-J. Effect of morphology of $\alpha - MnO_2$ nanocrystals on electrochemical detection of toxic metal ions. *Electrochem. Commun.* **2013**, *34*, 270 – 273.

(8) Xu, R. X.; Yu, X. Y.; Gao, C.; Jiang, Y. J.; Han, D. D.; Liu, J. H.; Huang, X. J. Non-conductive nanomaterial enhanced electrochemical response in stripping voltammetry: The use of nanostructured magnesium silicate hollow spheres for heavy metal ions detection. *Anal. Chim. Acta* **2013**, *790*, 31 – 38.

(9) Liu, Z.-G.; Chen, X.; Liu, J.-H.; Huang, X.-J. Well-arranged porous Co_3O_4 microsheets for electrochemistry of Pb(II) revealed by stripping voltammetry. *Electrochem. Commun.* **2013**, *30*, 59 – 62.

(10) Herzog, G.; Vodolazkaya, N. A.; Walcarius, A. Platinum Ultramicroelectrodes Modified with Electrogenerated Surfactant-Templated Mesoporous Organosilica Films: Effect of Film Formation Conditions on Its Performance in Preconcentration Electroanalysis. *Electroanal* **2013**, *25*, 2595–2603.

(11) Mbouguen, J. C. K.; Kenfack, I. T.; Walcarius, A.; Ngameni, E. Electrochemical response of ascorbic and uric acids at organoclay film modified glassy carbon electrodes and sensing applications. *Talanta* **2011**, *85*, 754 – 762.

(12) Tonlé, I. K.; Letaief, S.; Ngameni, E.; Walcarius, A.; Detellier, C. Square Wave Voltammetric Determination of Lead(II) Ions Using a Carbon Paste Electrode Modified by a Thiol-Functionalized Kaolinite. *Electroanal* **2011**, *23*, 245–252.

(13) Gong, J.; Zhang, W.; Liu, T.; Zhang, L. Facile fabrication of chitosan-calcium carbonate nanowall arrays and their use as a sensitive non-enzymatic organophosphate pesticide sensor. *Nanoscale* **2011**, *3*, 3123–3131.

(14) Zhang, Y.; Liu, Y.; Ji, X.; Banks, C. E.; Zhang, W. Flower-like hydroxyapatite modified carbon paste electrodes applicable for highly sensitive detection of heavy metal ions. *J. Mater. Chem.* **2011**, *21*, 7552–7554.

(15) Yin, Z.; Wu, J.; Yang, Z. A sensitive mercury (II) sensor based on CuO nanoshuttles/poly(thionine) modified glassy carbon electrode. *Microchim. Acta* **2010**, *170*, 307–312.

(16) Eloul, S.; Compton, R. G. Shielding of a Microdisc Electrode Surrounded by an Adsorbing Surface. *ChemElectroChem* **2014**, *1*, 917–924.

(17) Ellison, J.; Batchelor-McAuley, C.; Tschulik, K.; Compton, R. G. The use of cylindrical micro-wire electrodes for nano-impact experiments; facilitating the sub-picomolar detection of single nanoparticles. *Sensor. Actuat. B - Chem.* **2014**, *200*, 47 – 52.

(18) Tschulik, K.; Batchelor-McAuley, C.; Toh, H.-S.; Stuart, E. J. E.; Compton, R. G. Electrochemical studies of silver nanoparticles: a guide for experimentalists and a perspective. *Phys. Chem. Chem. Phys.* **2014**, *16*, 616–623.

(19) Zhou, Y. G.; Rees, N. V.; Compton, R. G. The Electrochemical Detection and Characterization of Silver Nanoparticles in Aqueous Solution. *Angwe. Chem. Int. Edit.* **2011**, *50*, 4219–4221.

(20) Liu, H.; Li, Y.; Sun, K.; Fan, J.; Zhang, P.; Meng, J.; Wang, S.; Jiang, L. Dual-Responsive Surfaces Modified with Phenylboronic Acid-Containing Polymer Brush To Reversibly Capture and Release Cancer Cells. *J. Am. Chem. Soc.* **2013**, *135*, 7603–7609.

(21) Kätelhön, E.; Krause, K. J.; Mathwig, K.; Lemay, S. G.; Wolfrum, B. Noise Phenomena Caused by Reversible Adsorption in Nanoscale Electrochemical Devices. *ACS Nano* **2014**, *8*, 4924–4930.

(22) Langmuir, I. The adsorption of gases on plane surfaces of glass, mica and platinum. *J. Am. Chem. Soc.* **1918**, *40*, 1361–1403.

(23) Barnes, E. O.; Compton, R. G. The rate of adsorption of nanoparticles on microelectrode surfaces. *J. Electroanal. Chem.* **2013**, *693*, 73–78.

(24) Brenner, H. The slow motion of a sphere through a viscous fluid towards a plane surface. *Chem. Eng. Sci.* **1961**, *16*, 242–251.

(25) Cutress, I. J.; Compton, R. G. How many molecules are required to measure a cyclic voltammogram? *Chem. Phys. Lett.* **2011**, *508*, 306–313.

(26) Cutress, I. J.; Dickinson, E. J.; Compton, R. G. Electrochemical random-walk theory: Probing voltammetry with small numbers of molecules: Stochastic versus statistical (Fickian) diffusion. *J. Electroanal. Chem.* **2011**, *655*, 1–8.

(27) Ward, K. R.; Lawrence, N. S.; Hartshorne, R. S.; Compton, R. G. Modelling the steady state voltammetry of a single spherical nanoparticle on a surface. *J. Electroanal. Chem.* **2012**, *683*, 37–42.

(28) Streeter, I.; Compton, R. G. Diffusion-Limited Currents to Nanoparticles of Various Shapes Supported on an Electrode; Spheres, Hemispheres, and Distorted Spheres and Hemispheres. *J. Phys. Chem. C* **2007**, *111*, 18049–18054.

(29) Crank, J. *The mathematics of diffusion*; Oxford university press: London, UK, 1979.

(30) Compton, R. G.; Pritchard, K. L. Kinetics of the Langmuirian adsorption of Cu^{II} ions at the calcite/water interface. *J. Chem. Soc., Faraday Trans.* **1990**, *86*, 129–136.

(31) Einstein, A. Über die von der molekularkinetischen Theorie der Wärme geforderte Bewegung von in ruhenden Flüssigkeiten suspendierten Teilchen. *Ann. Phys.* **1905**, *322*, 549–560.

(32) Gavaghan, D. An exponentially expanding mesh ideally suited to the fast and efficient simulation of diffusion processes at microdisc electrodes. 2. Application to chronoamperometry. *J. Electroanal. Chem.* **1998**, *456*, 13–23.

(33) Crank, J.; Nicolson, P. A practical method for numerical evaluation of solutions of partial differential equations of the heat-conduction type. Math. Proc. Cambridge; Cambridge University Press. 1947; pp 50–67.

(34) Compton, R. G.; Laborda, E.; Ward, K. R. *Understanding Voltammetry - Simulation of Electrode Processes*; Imperial College Press, 2013.

(35) Amatore, C.; Arbault, S.; Bonifas, I.; Guille, M. Quantitative investigations of amperometric spike feet suggest different controlling factors of the fusion pore in exocytosis at chromaffin cells. *Biophys. Chem.* **2009**, *143*, 124 – 131.

(36) Shoup, D.; Szabo, A. Chronoamperometric current at finite disk electrodes. *J. Electroanal. Chem. Interfacial Electrochem.* **1982**, *140*, 237–245.

Graphical TOC Entry